Double-Lepton Polarization Asymmetries and Branching Ratio of the $B \to \gamma l^+ l^-$ transition in Universal Extra Dimension

K. Azizi[1] *, N. K. Pak[2] †, B. B. Şirvanlı[3‡]

[1] Department of Physics, Doğuş University, Acıbadem-Kadıköy, 34722 Istanbul, Turkey

[2] Department of Physics, Middle East Technical University, 06800 Ankara, Turkey

[3] Department of Physics, Gazi University, Teknikokullar, 06100 Ankara, Turkey

Abstract

We study the radiative dileptonic $B \to \gamma l^+ l^-$ transition in the presence of a universal extra dimension in the Applequist-Cheng-Dobrescu model. In particular, using the corresponding form factors calculated via light cone QCD sum rules, we analyze the branching ratio and double lepton polarization asymmetries related to this channel and compare the results with the predictions of the standard model. We show how the results deviate from predictions of the standard model at lower values of the compactification factor $(1/R)$ of extra dimension.

PACS number(s): 12.60-i, 13.20.-v, 13.20.He

*e-mail: kazizi@dogus.edu.tr
†e-mail:pak@metu.edu.tr
‡e-mail:bbelma@gazi.edu.tr

1 Introduction

Although the standard model (SM) of particle physics is in perfect agreement with all confirmed collider data, there are some problems that can not be addressed by the SM. Some of these problems are matter-antimatter asymmetry, number of generations, unification of the fundamental interactions, etc. Hence, we need more fundamental theories beyond the SM (BSM) such that at low energies those theories reduce to the SM. One of the most interesting candidates as a BSM theory is extra dimension (ED) [1–6]. A kind of ED which permits both gauge bosons and fermions as SM fields to spread in ED's is labeled as universal extra dimension (UED). The simplest case of the UED is the Applequist-Cheng-Dobrescu (ACD) model [7] which contains only one UED compactified in a circle of radius R.

We have no experimental evidence for the new physics effects such as ED's so far, but we expect that the LHC will open new horizons in this respect. There are two alternative ways to search for ED's. In direct search, we look for Kaluza-Klein (KK) excitations directly by increasing the center of mass energy of colling particles. In indirect search, we look for the contributions of the KK particles to the hadronic decay channels. The flavor changing neutral current (FCNC) transitions induced by loop level quark transitions are considered as good tools for studying the KK effects.

The ACD model has been previously applied to many rare semileptonic decay channels [8–17]. In the present work, we apply this model to analyze the branching ratio and double lepton polarization asymmetries defining the radiative dileptonic $B \to \gamma l^+ l^-$ transition. The advantage of such decay channel compared to the pure leptonic helicity suppressed $B \to \mu^+\mu^-$ and $B \to e^+e^-$ channels is that due to the emission of the photon in addition to the lepton pair, we have no helicity suppression here and we expect larger branching ratio [18, 19]. The upper experimental limits, $Br(B \to \mu^+\mu^-) < 1.5 \times 10^{-8}$, $Br(B \to \gamma\mu^+\mu^-) < 1.6 \times 10^{-7}$, $Br(B \to e^+e^-) < 8.3 \times 10^{-8}$, $Br(B \to \gamma e^+e^-) < 1.2 \times 10^{-7}$ [20] verify our expectations in this respect. The considered decay channel proceeds via FCNC transition of $b \to d l^+ l^-$ at quark level and as we previously mentioned the KK particles can contribute to such channels. To evaluate the branching ratio and various double lepton polarization asymmetries, we will use the form factors entering the effective Hamiltonian calculated via light cone QCD sum rules [18, 21–23].

The layout of the paper is as follows. The introduction is followed by section 2 which encompasses the theoretical background of the decay channel under consideration and the associated effective Hamiltonian, a brief review on the ACD model, transition matrix ele-

ments defining the radiative dileptonic $B \to \gamma l^+ l^-$ decay channel and explicit expressions for the associated observables (differential decay rate and double lepton polarization asymmetries) in the UED model. In section 3, using the fit parametrization of form factors as the main ingredients as well as other input parameters, we numerically analyze the physical observables both in the UED and the SM models and discuss how the results obtained from the UED model deviate from those of the SM.

2 The radiative dileptonic $B \to \gamma l^+ l^-$ transition in the ACD model

As we mentioned in the previous section, the $B \to \gamma l^+ l^-$ transition proceeds via the FCNC transition of the $b \to d l^+ l^-$ at the quark level. The most important contribution to the $B \to \gamma l^+ l^-$ comes from the pure leptonic $B \to l^+ l^-$ transition. The latter proceeds via the box and Z-photon mediated penguin diagrams (see for instance [18, 19]). By attaching the photon to any external and internal charged lines, we will obtain the transition matrix elements for the $B \to \gamma l^+ l^-$ decay. In the SM, the effective Hamiltonian responsible for $b \to q \ell^+ \ell^-$ transition can be written as

$$\mathcal{H}_{eff} = \frac{\alpha G_F}{\sqrt{2}\pi} V_{tb} V_{td}^* \Bigg[C_9^{eff} (\bar{d}\gamma_\mu P_L b)\bar{l}\gamma_\mu l + C_{10} \bar{d}\gamma_\mu P_L b \bar{l}\gamma_\mu \gamma_5 l - 2\frac{C_7^{eff}}{q^2} \bar{d} i\sigma_{\mu\nu} q_\nu (m_b P_R + m_d P_L) b \bar{l}\gamma_\mu l \Bigg], \tag{2.1}$$

where $P_{R(L)} = \frac{1+(-)\gamma_5}{2}$, and q^2 is the transferred momentum squared. The C_7^{eff}, C_9^{eff} and C_{10} are Wilson coefficients which are the source of difference between the SM and UED models. In the UED, the form of Hamiltonian remains unchanged; however, the Wilson coefficients are modified [24–28] as a result of interactions of the KK particles with each other as well as with the usual SM particles. In this model, each Wilson coefficient is written in terms of the ordinary SM part and an extra part coming from the aforementioned interactions. Hence,

$$F(x_t, 1/R) = F_0(x_t) + \sum_{n=1}^{\infty} F_n(x_t, x_n), \tag{2.2}$$

where $F_0(x_t)$ is the SM part and $x_t = m_t^2/M_W^2$ with m_t and M_W being masses of the top quark and the W boson, respectively. The second part is defined in terms of the compactification factor $1/R$ via

$$x_n = m_n^2/m_W^2, \qquad \text{with} \qquad m_n = n/R, \tag{2.3}$$

where m_n is mass of the KK particles and $n = 0$ corresponds to the ordinary SM particles. Here we should also mention that the KK sums appearing in all Wilson coefficients converge and give finite results.

Now, we proceed to present the explicit expressions of the Wilson coefficients entering the low energy effective Hamiltonian obtained by a renormalization group evolution from the electroweak scale down to the m_b scale. In the leading log approximation, the coefficient $C_7^{eff}(1/R)$ is written as [24–28]:

$$C_7^{eff}(\mu_b, 1/R) = \eta^{\frac{16}{23}} C_7(\mu_W, 1/R) + \frac{8}{3}\left(\eta^{\frac{14}{23}} - \eta^{\frac{16}{23}}\right) C_8(\mu_W, 1/R) + C_2(\mu_W) \sum_{i=1}^{8} h_i \eta^{a_i} \ , \tag{2.4}$$

where

$$\eta = \frac{\alpha_s(\mu_W)}{\alpha_s(\mu_b)} \ , \tag{2.5}$$

and

$$\alpha_s(x) = \frac{\alpha_s(m_Z)}{1 - \beta_0 \frac{\alpha_s(m_Z)}{2\pi} \ln(\frac{m_Z}{x})}, \tag{2.6}$$

with $\alpha_s(m_Z) = 0.118$ and $\beta_0 = \frac{23}{3}$. The coefficients a_i and h_i, with i running from 1 to 8, are also given as [27, 28]:

$$\begin{aligned} a_i &= (\ \ \tfrac{14}{23}, \ \ \ \tfrac{16}{23}, \ \tfrac{6}{23}, \ -\tfrac{12}{23}, \ \ 0.4086, \ -0.4230, \ -0.8994, \ \ 0.1456\ ), \\ h_i &= (\ 2.2996, \ -1.0880, \ -\tfrac{3}{7}, \ -\tfrac{1}{14}, \ -0.6494, \ -0.0380, \ -0.0186, \ -0.0057\ ). \end{aligned} \tag{2.7}$$

The functions

$$C_2(\mu_W) = 1 \ , \quad C_7(\mu_W, 1/R) = -\frac{1}{2} D'(x_t, 1/R) \ , \quad C_8(\mu_W, 1/R) = -\frac{1}{2} E'(x_t, 1/R) \ . \tag{2.8}$$

Also, the $1/R$ -dependent functions $D'(x_t, 1/R)$ and $E'(x_t, 1/R)$ are defined as

$$D'(x_t, 1/R) = D'_0(x_t) + \sum_{n=1}^{\infty} D'_n(x_t, x_n), \qquad E'(x_t, 1/R) = E'_0(x_t) + \sum_{n=1}^{\infty} E'_n(x_t, x_n) \ , \tag{2.9}$$

where the SM parts are given as

$$D'_0(x_t) = -\frac{(8x_t^3 + 5x_t^2 - 7x_t)}{12(1 - x_t)^3} + \frac{x_t^2(2 - 3x_t)}{2(1 - x_t)^4} \ln x_t \ , \tag{2.10}$$

$$E'_0(x_t) = -\frac{x_t(x_t^2 - 5x_t - 2)}{4(1 - x_t)^3} + \frac{3x_t^2}{2(1 - x_t)^4} \ln x_t \ , \tag{2.11}$$

and the parts coming from the new interactions can be written in the forms

$$\begin{aligned}
&\sum_{n=1}^{\infty} D'_n(x_t, x_n) \\
&= \frac{x_t[37 - x_t(44 + 17x_t)]}{72(x_t - 1)^3} + \frac{\pi m_W R}{12}\Bigg[\int_0^1 dy\,(2y^{1/2} + 7y^{3/2} + 3y^{5/2})\,\coth(\pi m_W R\sqrt{y}) \\
&- \frac{x_t(2 - 3x_t)(1 + 3x_t)}{(x_t - 1)^4} J(R, -1/2) - \frac{1}{(x_t - 1)^4}\Big\{x_t(1 + 3x_t) + (2 - 3x_t)[1 - (10 - x_t)x_t]\Big\} \\
&\times \quad J(R, 1/2) - \frac{1}{(x_t - 1)^4}[(2 - 3x_t)(3 + x_t) + 1 - (10 - x_t)x_t] J(R, 3/2) - \frac{(3 + x_t)}{(x_t - 1)^4} J(R, 5/2)\Bigg]\,,
\end{aligned} \tag{2.12}$$

and

$$\begin{aligned}
&\sum_{n=1}^{\infty} E'_n(x_t, x_n) \\
&= \frac{x_t[17 + (8 - x_t)x_t]}{24(x_t - 1)^3} + \frac{\pi m_W R}{4}\Bigg[\int_0^1 dy\,(y^{1/2} + 2y^{3/2} - 3y^{5/2})\,\coth(\pi m_W R\sqrt{y}) \\
&- \frac{x_t(1 + 3x_t)}{(x_t - 1)^4} J(R, -1/2) + \frac{1}{(x_t - 1)^4}[x_t(1 + 3x_t) - 1 + (10 - x_t)x_t] J(R, 1/2) \\
&- \frac{1}{(x_t - 1)^4}[(3 + x_t) - 1 + (10 - x_t)x_t)] J(R, 3/2) + \frac{(3 + x_t)}{(x_t - 1)^4} J(R, 5/2)\Bigg]\,.
\end{aligned} \tag{2.13}$$

Here,

$$J(R, \alpha) = \int_0^1 dy\, y^{\alpha}\left[\coth(\pi m_W R\sqrt{y}) - x_t^{1+\alpha}\coth(\pi m_t R\sqrt{y})\right]\,. \tag{2.14}$$

The next Wilson coefficient is C_9^{eff}. In the leading log approximation and at μ_b scale it is given as [27, 28]:

$$\begin{aligned}
C_9^{eff}(\mu_b, \hat{s}', 1/R) \;=\; & C_9^{NDR}(1/R)\eta(\hat{s}') + h(z, \hat{s}')\,(3C_1 + C_2 + 3C_3 + C_4 + 3C_5 + C_6) \\
& -\frac{1}{2}h(1, \hat{s}')\,(4C_3 + 4C_4 + 3C_5 + C_6) \\
& -\frac{1}{2}h(0, \hat{s}')\,(C_3 + 3C_4) + \frac{2}{9}\,(3C_3 + C_4 + 3C_5 + C_6)\,,
\end{aligned} \tag{2.15}$$

where, $\hat{s}' = \frac{q^2}{m_b^2}$ with the physical region $4m_l^2 \le q^2 \le m_B^2$. The function $C_9^{NDR}(1/R)$ in the naive dimensional regularization (NDR) scheme is defined as

$$C_9^{NDR}(1/R) \;=\; P_0^{NDR} + \frac{Y(x_t)}{\sin^2\theta_W} - 4Z(x_t) + P_E E(x_t). \tag{2.16}$$

Here we should underline that, due to smallness of P_E, we can neglect the contribution of last term in Eq. (2.16). The constant $P_0^{NDR} = 2.60 \pm 0.25$ [27, 28], and remaining two functions $Y(x_t, 1/R)$ and $Z(x_t, 1/R)$ have the following expressions:

$$Y(x_t, 1/R) = Y_0(x_t) + \sum_{n=1}^{\infty} C_n(x_t, x_n) \ , \tag{2.17}$$

where,

$$Y_0(x_t) = \frac{x_t}{8}\left[\frac{x_t - 4}{x_t - 1} + \frac{3x_t}{(x_t-1)^2}\ln x_t\right] \ , \tag{2.18}$$

and,

$$\sum_{n=1}^{\infty} C_n(x_t, x_n) = \frac{x_t(7-x_t)}{16(x_t-1)} - \frac{\pi m_W R x_t}{16(x_t-1)^2}\left[3(1+x_t)J(R,-1/2) + (x_t-7)J(R,1/2)\right] \ . \tag{2.19}$$

also

$$Z(x_t, 1/R) = Z_0(x_t) + \sum_{n=1}^{\infty} C_n(x_t, x_n) \ , \tag{2.20}$$

with

$$Z_0(x_t) = \frac{18x_t^4 - 163x_t^3 + 259x_t^2 - 108x_t}{144(x_t-1)^3} + \left[\frac{32x_t^4 - 38x_t^3 - 15x_t^2 + 18x_t}{72(x_t-1)^4} - \frac{1}{9}\right]\ln x_t. \tag{2.21}$$

To complete the presentation of the coefficient C_9^{eff} in Eq. (2.15), we define

$$\eta(\hat{s}') \ = \ 1 + \frac{\alpha_s(\mu_b)}{\pi}\,\omega(\hat{s}'), \tag{2.22}$$

where,

$$\begin{aligned}\omega(\hat{s}') \ = \ & -\frac{2}{9}\pi^2 - \frac{4}{3}\mathrm{Li}_2(\hat{s}') - \frac{2}{3}(\ln\hat{s}')\ln(1-\hat{s}') - \frac{5+4\hat{s}'}{3(1+2\hat{s}')}\ln(1-\hat{s}') - \\ & \frac{2\hat{s}'(1+\hat{s}')(1-2\hat{s}')}{3(1-\hat{s}')^2(1+2\hat{s}')}\ln\hat{s}' + \frac{5+9\hat{s}'-6\hat{s}'^2}{6(1-\hat{s}')(1+2\hat{s}')}.\end{aligned} \tag{2.23}$$

The coefficients C_j $(j = 1, ...6)$ are given as

$$C_j = \sum_{i=1}^{8} k_{ji}\eta^{a_i} \qquad (j = 1, ...6) \tag{2.24}$$

and the constants k_{ji} have the values

$$\begin{aligned}
k_{1i} &= (\ 0,\ \ 0,\ \ \tfrac{1}{2},\ \ -\tfrac{1}{2},\ \ 0,\ \ 0,\ \ 0,\ \ 0\ ),\\
k_{2i} &= (\ 0,\ \ 0,\ \ \tfrac{1}{2},\ \ \tfrac{1}{2},\ \ 0,\ \ 0,\ \ 0,\ \ 0\ ),\\
k_{3i} &= (\ 0,\ \ 0,\ \ -\tfrac{1}{14},\ \ \tfrac{1}{6},\ \ 0.0510,\ \ -0.1403,\ \ -0.0113,\ \ 0.0054\ ),\\
k_{4i} &= (\ 0,\ \ 0,\ \ -\tfrac{1}{14},\ \ -\tfrac{1}{6},\ \ 0.0984,\ \ 0.1214,\ \ 0.0156,\ \ 0.0026\ ),\\
k_{5i} &= (\ 0,\ \ 0,\ \ 0,\ \ 0,\ \ -0.0397,\ \ 0.0117,\ \ -0.0025,\ \ 0.0304\ ),\\
k_{6i} &= (\ 0,\ \ 0,\ \ 0,\ \ 0,\ \ 0.0335,\ \ 0.0239,\ \ -0.0462,\ \ -0.0112\ ).
\end{aligned} \tag{2.25}$$

Finally, we should define the other functions in Eq. (2.15):

$$h(y,\hat{s}') = -\frac{8}{9}\ln\frac{m_b}{\mu_b} - \frac{8}{9}\ln y + \frac{8}{27} + \frac{4}{9}x \tag{2.26}$$

$$-\frac{2}{9}(2+x)|1-x|^{1/2}\begin{cases} \left(\ln\left|\frac{\sqrt{1-x}+1}{\sqrt{1-x}-1}\right| - i\pi\right), & \text{for } x \equiv \frac{4z^2}{\hat{s}'} < 1 \\ 2\arctan\frac{1}{\sqrt{x-1}}, & \text{for } x \equiv \frac{4z^2}{\hat{s}'} > 1, \end{cases} \tag{2.27}$$

where $y = 1$ or $y = z = \frac{m_c}{m_b}$ and,

$$h(0,\hat{s}') = \frac{8}{27} - \frac{8}{9}\ln\frac{m_b}{\mu_b} - \frac{4}{9}\ln\hat{s}' + \frac{4}{9}i\pi. \tag{2.28}$$

The Wilson coefficient C_{10} is scale-independent and is given as:

$$C_{10}(1/R) = -\frac{Y(x_t, 1/R)}{\sin^2\theta_W}\ , \tag{2.29}$$

where, $\sin^2\theta_W = 0.23$.

Once the Wilson coefficients in UED model are specified explicitly, we proceed to obtain the amplitude for the decay channel under consideration which is obtained by sandwiching the effective Hamiltonian between the final photon and the initial B meson state. As previously noted, the diagrams defining the $B \to \gamma l^+ l^-$ transition are obtained attaching the photon to any external and internal charged lines. Hence, we have three kinds of contributions: 1) the photon is emitted from the initial quark lines, 2) the photon is radiated from the final charged lepton lines and 3) the photon is attached to any charged internal line. When photon is attached to the initial quark lines (structure dependent part), the $B \to \gamma l^+ l^-$ transition is described by three Wilson coefficients C_7^{eff}, C_9^{eff} and C_{10} and we deal with the long distance effects. Therefore, the amplitude is written as

$$M_1 = \langle\gamma(k)|\mathcal{H}_{eff}|B(p)\rangle \tag{2.30}$$

where k is the momentum of the photon and the $p = k + q$ is the initial momentum. To obtain the amplitude M_1, we need to define the matrix elements

$$\left\langle \gamma(k) \left| \bar{d}\gamma_\mu(1-\gamma_5)b \right| B(p) \right\rangle = \frac{e}{m_B^2}\Big\{\epsilon_{\mu\nu\lambda\sigma}\varepsilon^{*\nu}q^\lambda k^\sigma g(q^2) + i\left[\varepsilon_\mu^*(kq) - (\varepsilon^* q)k_\mu\right]f(q^2)\Big\} \ , \tag{2.31}$$

and

$$\left\langle \gamma(k) \left| \bar{d}i\sigma_{\mu\nu}q^\nu(1+\gamma_5)b \right| B(p) \right\rangle = \frac{e}{m_B^2}\Big\{\epsilon_{\mu\nu\lambda\sigma}\,\varepsilon^{\nu *}q^\lambda k^\sigma g_1(q^2) + i\left[\varepsilon_\mu^*(qk) - (\varepsilon^* q)k_\mu\right]f_1(q^2)\Big\} \ , \tag{2.32}$$

where ε_μ^* is the four vector polarization of the photon, and $g(q^2)$, $f(q^2)$, $g_1(q^2)$ and $f_1(q^2)$ are the transition form factors.

When photon is radiated from the final charged leptons (Bremsstrahlung part) the corresponding amplitude is called M_2. From the helicity arguments it follows that the amplitude M_2 should be proportional to the lepton mass m_l; for the cases of the $l = e,\ \mu$ we can safely ignore from such contributions. For τ lepton case, this amplitude is calculated in [19]. Finally, when the photon is attached to any charged internal line, the amplitude of such contributions (M_3) is proportional to $\frac{m_b^2}{m_W^2}$; so these contributions for all leptons are strongly suppressed and we can safely ignore those contributions (see for instance [18, 19]).

Now we proceed to present the $1/R$-dependent physical observables defining the radiative dileptonic $B \to \gamma l^+ l^-$ transition. Considering the aforementioned contributions, the differential decay rate for the $l = e$ or μ case as a function of the compactification factor is obtained as [18]:

$$\begin{aligned}\frac{d\Gamma}{d\hat{s}}(\hat{s}, 1/R) &= \frac{\alpha^3 G_F^2}{768\pi^5}\left|V_{tb}V_{td}^*\right|^2 m_B^5 \hat{s}(1-\hat{s})^3\sqrt{1-4\frac{\hat{m}_l{}^2}{\hat{s}}}\times \\ &\times\left\{\frac{1}{m_B^2}\left[|A|^2+|B|^2\right] + \frac{1}{m_B^2}\left|C_{10}(1/R)\right|^2\left[f^2(q^2)+g^2(q^2)\right]\right\} \ , \end{aligned} \tag{2.33}$$

where $\hat{s} = \frac{q^2}{m_B^2}$, $\hat{m}_l = \frac{m_l}{m_B}$,

$$\begin{aligned} A = A(\hat{s}, 1/R) &= C_9^{eff}(\hat{s}, 1/R)g(q^2) - 2\,C_7^{eff}(1/R)\frac{m_b}{\hat{s}m_B^2}g_1(q^2) \ , \\ &\text{and} \\ B = B(\hat{s}, 1/R) &= C_9^{eff}(\hat{s}, 1/R)f(q^2) - 2\,C_7^{eff}(1/R)\frac{m_b}{\hat{s}m_B^2}f_1(q^2) \ . \end{aligned}$$

In the case of τ, the differential decay width is obtained as [19]:

$$\frac{d\Gamma}{d\hat{s}}(\hat{s},1/R) = \left|\frac{\alpha G_F}{2\sqrt{2}\,\pi}V_{tb}V_{td}^*\right|^2 \frac{\alpha}{(2\,\pi)^3}\,m_B^5\pi\Bigg\{\frac{1}{12}\int_\delta^{1-4r} x^3\,dx\,\sqrt{1-\frac{4r}{1-x}}\,m_B^2\Bigg[\Big(|A'|^2+|B'|^2\Big)(1-x+2r)$$
$$+\Big(|C|^2+|D|^2\Big)(1-x-4r)\Bigg] - 2C_{10}(1/R)f_B r\int_\delta^{1-4r} x^2\,dx\,\mathrm{Re}\,(A')\,\ln\frac{1+\sqrt{1-\frac{4r}{1-x}}}{1-\sqrt{1-\frac{4r}{1-x}}}$$
$$-4\,|f_B\;C_{10}(1/R)|^2\,r\,\frac{1}{m_B^2}\int_\delta^{1-4r} dx\Bigg[\left(2+\frac{4r}{x}-\frac{2}{x}-x\right)\ln\frac{1+\sqrt{1-\frac{4r}{1-x}}}{1-\sqrt{1-\frac{4r}{1-x}}}$$
$$+\frac{2}{x}\,(1-x)\,\sqrt{1-\frac{4r}{1-x}}\Bigg]\Bigg\}\,, \tag{2.34}$$

where the f_B is the leptonic decay constant of the B meson, $x=\dfrac{2E_\gamma}{m_B}$ is a dimensionless parameter with E_γ being the photon energy and $r=\dfrac{m_\tau^2}{m_B^2}$. The lower limit of integration over x comes from imposing a cut on the photon energy (for details see [19]). Considering the experimental cut imposed on the minimum energy for detectable photon, we demand the energy of the photon to be larger than 50 MeV, i.e., $E_\gamma \geq a\,m_B$ with $a \geq 0.01$. As a result, the lower limit is set as $\delta = 2a$ and we will take $\delta = 0.02$ for the lower limit of integration over x. In Eq. (2.34), we have introduced the following coefficients:

$$\begin{aligned}
A' = A'(\hat{s},1/R) &= \frac{A(\hat{s},1/R)}{m_B^2}\,,\\
B' = B'(\hat{s},1/R) &= \frac{B(\hat{s},1/R)}{m_B^2}\,,\\
C = C(1/R) &= \frac{C_{10}(1/R)}{m_B^2}\,g(q^2)\,,\\
D = D(1/R) &= \frac{C_{10}(1/R)}{m_B^2}\,f(q^2)\,.
\end{aligned} \tag{2.35}$$

At the end of this section we would like to present various $1/R$-dependent double–lepton polarization asymmetries for the transition under study. Note that using the most general model-independent form of the effective Hamiltonian including all possible forms of the interactions, these double–lepton polarization asymmetries are calculated in the [29]. To calculate the double–polarization asymmetries in our case, we consider the polarizations

of both lepton and anti-lepton, simultaneously and suggest the following spin projection operators for the lepton ℓ^- and the anti-lepton ℓ^+:

$$\begin{aligned}\Lambda_1 &= \frac{1}{2}(1+\gamma_5 \not{s}_i^-) \ , \\ \Lambda_2 &= \frac{1}{2}(1+\gamma_5 \not{s}_i^+) \ ,\end{aligned} \tag{2.36}$$

where $i = L, N$ and T correspond to the longitudinal, normal and transversal polarizations, respectively. Then, we introduce the following orthogonal vectors s^μ in the rest frame of the lepton and anti-lepton:

$$\begin{aligned}s_L^{-\mu} &= \left(0, \vec{e}_L^{\,-}\right) = \left(0, \frac{\vec{p}_1}{|\vec{p}_1|}\right) \ , \\ s_N^{-\mu} &= \left(0, \vec{e}_N^{\,-}\right) = \left(0, \frac{\vec{k}\times\vec{p}_1}{\left|\vec{k}\times\vec{p}_1\right|}\right) \ , \\ s_T^{-\mu} &= \left(0, \vec{e}_T^{\,-}\right) = \left(0, \vec{e}_N^{\,-}\times\vec{e}_L^{\,-}\right) \ , \\ s_L^{+\mu} &= \left(0, \vec{e}_L^{\,+}\right) = \left(0, \frac{\vec{p}_2}{|\vec{p}_2|}\right) \ , \\ s_N^{+\mu} &= \left(0, \vec{e}_N^{\,+}\right) = \left(0, \frac{\vec{k}\times\vec{p}_2}{\left|\vec{k}\times\vec{p}_2\right|}\right) \ , \\ s_T^{+\mu} &= \left(0, \vec{e}_T^{\,+}\right) = \left(0, \vec{e}_N^{\,+}\times\vec{e}_L^{\,+}\right) \ ,\end{aligned} \tag{2.37}$$

where $\vec{p}_{1(2)}$ are the three–momenta of the leptons $\ell^{-(+)}$ and $\vec{k}$ is three-momentum of the final photon in the center of mass (CM) frame of $\ell^-\,\ell^+$. The longitudinal unit vectors are boosted to the CM frame of $\ell^-\ell^+$ via Lorenz transformations

$$\begin{aligned}\left(s_L^{-\mu}\right)_{CM} &= \left(\frac{|\vec{p}_1|}{m_\ell}\ , \frac{E\vec{p}_1}{m_\ell\,|\vec{p}_1|}\right) \ , \\ \left(s_L^{+\mu}\right)_{CM} &= \left(\frac{|\vec{p}_1|}{m_\ell}\ , -\frac{E\vec{p}_1}{m_\ell\,|\vec{p}_1|}\right) \ ,\end{aligned} \tag{2.38}$$

while the other two vectors remain unchanged. Finally, we define the double–lepton polarization asymmetries as:

$$P_{ij}(\hat{s}) = \frac{\left(\frac{d\Gamma}{d\hat{s}}(\vec{s}_i^{\,-}, \vec{s}_j^{\,+}) - \frac{d\Gamma}{d\hat{s}}(-\vec{s}_i^{\,-}, \vec{s}_j^{\,+})\right) - \left(\frac{d\Gamma}{d\hat{s}}(\vec{s}_i^{\,-}, -\vec{s}_j^{\,+}) - \frac{d\Gamma}{d\hat{s}}(-\vec{s}_i^{\,-}, -\vec{s}_j^{\,+})\right)}{\left(\frac{d\Gamma}{d\hat{s}}(\vec{s}_i^{\,-}, \vec{s}_j^{\,+}) + \frac{d\Gamma}{d\hat{s}}(-\vec{s}_i^{\,-}, \vec{s}_j^{\,+})\right) + \left(\frac{d\Gamma}{d\hat{s}}(\vec{s}_i^{\,-}, -\vec{s}_j^{\,+}) + \frac{d\Gamma}{d\hat{s}}(-\vec{s}_i^{\,-}, -\vec{s}_j^{\,+})\right)} \ , \tag{2.39}$$

where the subindex j also stands for the L, N or T polarization. The subindexses, i and j correspond to the lepton and anti-lepton, respectively. Using the above definitions, the various $1/R$-dependent double lepton polarization asymmetries are obtained as:

$$
\begin{aligned}
P_{LL}(\hat{s},1/R) = & \frac{1}{\Delta(\hat{s},1/R)} \\
\times & \left\{ \frac{1}{2} f_B^2 m_B^4 \Big\{ (1-\hat{s})^2(\mathcal{I}_1+\mathcal{I}_4) - [2\hat{s}+(1+\hat{s}^2)v^2]\mathcal{I}_3 + [2\hat{s}-(1+\hat{s}^2)v^2]\mathcal{I}_6 \Big\} |F|^2 \right. \\
- & \frac{1}{2\hat{m}_\ell} f_B m_B \hat{s} \Big[8(1+\hat{s})v^2 + m_B^2(1-\hat{s})(2-2\hat{s}-2v^2+2\hat{s}v^2+v^4+\hat{s}v^4)\mathcal{I}_8 \\
- & m_B^2(1-\hat{s}^2)v^2\mathcal{I}_9 \Big] \mathrm{Re}[(A_1^*+B_1^*)F] - \frac{1}{3\hat{m}_\ell^2} m_B^2 \hat{s}^2(1-\hat{s})^2(1-v^2)^2 \mathrm{Re}[A_1^* B_1 + A_2^* B_2] \\
- & \left. \frac{2}{3} m_B^2 \hat{s}(1-\hat{s})^2(1+3v^2) \Big(|A_1|^2 + |A_2|^2 + |B_1|^2 + |B_2|^2 \Big) \right\} , \qquad (2.40)
\end{aligned}
$$

$$
\begin{aligned}
P_{LN}(\hat{s},1/R) = & \frac{1}{\Delta(\hat{s},1/R)} \left\{ f_B m_B^3 \sqrt{\hat{s}}(1-\hat{s}^2)v^2 \mathrm{Im}[A_1^* F - B_1^* F]\mathcal{I}_7 \right. \\
- & \left. 4\pi f_B m_B \sqrt{\hat{s}}(1-\hat{s})(1-\sqrt{1-v^2}) \mathrm{Im}[(A_2^*+B_2^*)F] \right\} , \qquad (2.41)
\end{aligned}
$$

$$
\begin{aligned}
P_{NL}(\hat{s},1/R) = & \frac{1}{\Delta(\hat{s},1/R)} \left\{ f_B m_B^3 \sqrt{\hat{s}}(1-\hat{s}^2)v^2 \mathrm{Im}[-A_1^* F + B_1^* F]\mathcal{I}_7 \right. \\
+ & \left. 4\pi f_B m_B \sqrt{\hat{s}}(1-\hat{s})(1-\sqrt{1-v^2}) \mathrm{Im}[-(A_2^*+B_2^*)F] \right\} , \qquad (2.42)
\end{aligned}
$$

$$
\begin{aligned}
P_{LT}(\hat{s},1/R) = & \frac{1}{\Delta(\hat{s},1/R)} \left\{ -\frac{1}{\sqrt{\hat{s}}} f_B^2 m_B^4 \hat{m}_\ell (1-\hat{s}) v \Big[(1+\hat{s})\,|F|^2 \Big] (\mathcal{I}_2+\mathcal{I}_4) \right. \\
+ & \frac{4}{v}\pi f_B m_B \sqrt{\hat{s}}(1-\hat{s})(1-\sqrt{1-v^2}) \mathrm{Re}[(A_2^*-B_2^*)F] + 2 m_B \hat{m}_\ell \mathrm{Re}[A_1^* A_2 - B_1^* B_2] \Big] \\
- & \left. \frac{4}{v}\pi f_B m_B \sqrt{\hat{s}}(1+\hat{s})(1-\sqrt{1-v^2}) \mathrm{Re}[(A_1^*+B_1^*)F] \Big] \right\} , \qquad (2.43)
\end{aligned}
$$

$$
\begin{aligned}
P_{TL}(\hat{s},1/R) = & \frac{1}{\Delta(\hat{s},1/R)} \left\{ -\frac{1}{\sqrt{\hat{s}}} f_B^2 m_B^4 \hat{m}_\ell (1-\hat{s}) v \Big[(1+\hat{s})\,|F|^2 \Big] (\mathcal{I}_2+\mathcal{I}_4) \right. \\
- & \frac{4}{v}\pi f_B m_B \sqrt{\hat{s}}(1-\hat{s})(1-\sqrt{1-v^2}) \mathrm{Re}[(A_2^*-B_2^*)F] - 2 m_B \hat{m}_\ell \mathrm{Re}[A_1^* A_2 - B_1^* B_2] \Big] \\
- & \left. \frac{4}{v}\pi f_B m_B \sqrt{\hat{s}}(1+\hat{s})(1-\sqrt{1-v^2}) \mathrm{Re}[(A_1^*+B_1^*)F] \Big] \right\} , \qquad (2.44)
\end{aligned}
$$

$$P_{NT}(\hat{s},1/R) = \frac{1}{\Delta(\hat{s},1/R)}\Bigg\{2f_B m_B^3 \hat{m}_\ell (1-\hat{s})^2 v\mathrm{Im}[-A_1^* F + B_1^* F](\mathcal{I}_8 - \mathcal{I}_9)$$
$$- \quad 2f_B m_B^3 \hat{m}_\ell (1-\hat{s}^2) v\mathrm{Im}[(A_2^* + B_2^*)F](\mathcal{I}_8 - \mathcal{I}_9)$$
$$- \quad \frac{8}{3} m_B (1-\hat{s})^2 v\mathrm{Im}[-m_B \hat{s}(A_1^* B_1 + A_2^* B_2)]\Bigg\}\,, \tag{2.45}$$

$$P_{TN}(\hat{s},1/R) = \frac{1}{\Delta(\hat{s},1/R)}\Bigg\{2f_B m_B^3 \hat{m}_\ell (1-\hat{s})^2 v\mathrm{Im}[A_1^* F - B_1^* F](\mathcal{I}_8 - \mathcal{I}_9)$$
$$- \quad 2f_B m_B^3 \hat{m}_\ell (1-\hat{s}^2) v\mathrm{Im}[(A_2^* + B_2^*)F](\mathcal{I}_8 - \mathcal{I}_9)$$
$$+ \quad \frac{8}{3} m_B (1-\hat{s})^2 v\mathrm{Im}[-m_B \hat{s}(A_1^* B_1 + A_2^* B_2)]\Bigg\}\,, \tag{2.46}$$

$$P_{NN}(\hat{s},1/R) = \frac{1}{\Delta(\hat{s},1/R)}\Bigg\{f_B^2 m_B^4 \hat{s}\Big[(1+v^2)\mathcal{I}_3 - (1-v^2)\mathcal{I}_6\Big]\,|F|^2$$
$$+ \quad \frac{4}{3} m_B^2 \hat{s}(1-\hat{s})^2 v^2 \Big(2\mathrm{Re}[A_1^* B_1 + A_2^* B_2]\Big)\Bigg\}\,, \tag{2.47}$$

$$P_{TT}(\hat{s},1/R) = \frac{1}{\Delta(\hat{s},1/R)}\Bigg\{\frac{1}{2} f_B^2 m_B^4 \Big\{ -(1-\hat{s})^2(1-v^2)\mathcal{I}_1 + [1 - v^2 - 4\hat{s} + \hat{s}^2(1-v^2)]\mathcal{I}_3$$
$$- (1-v^2)(1-\hat{s})^2 \mathcal{I}_4 + (1-v^2)(1-\hat{s}^2)\mathcal{I}_6\Big\}\,|F|^2$$
$$- 4f_B m_B^3 \hat{m}_\ell (1-\hat{s})^2 \mathrm{Re}[(A_1^* + B_1^*)F](\mathcal{I}_8 - \mathcal{I}_9)$$
$$+ \quad m_B \hat{m}_\ell \Big(|A_1|^2 + |A_2|^2 + |B_1|^2 + |B_1|^2\Big)\Big] + \frac{8}{3} m_B^2 (1-\hat{s})^2 \Big(\hat{s}\mathrm{Re}[A_1^* B_1 + A_2^* B_2]\Big)\Bigg\}\,, \tag{2.48}$$

where,

$$\Delta(\hat{s},1/R) = 16 m_B \hat{m}_\ell (1-\hat{s})^2 \Big(\mathrm{Re}[m_B \hat{m}_\ell (A_1^* B_1 + A_2^* B_1)]\Big)$$
$$+ \quad \frac{2}{3}(1-\hat{s})^2 \Big[m_B^2 \hat{s}(3+v^2)\Big(|A_1|^2 + |A_2|^2 + |B_1|^2 + |B_2|^2\Big)\Big]$$
$$- \quad \frac{1}{2} f_B^2 m_B^4 |F|^2 \Big\{(1-\hat{s})^2 v^2 (\mathcal{I}_1 + \mathcal{I}_4) - (1 + \hat{s}^2 + 2\hat{s}v^2)\mathcal{I}_3 - [1 - \hat{s}(4 - \hat{s} - 2v^2)]\mathcal{I}_6\Big\}$$
$$+ \quad 2f_B m_B \hat{m}_\ell \mathrm{Re}[(A_1^* + B_1^*)F]\Big[8(1+\hat{s}) + m_B^2(1-\hat{s}^2)v^2\mathcal{I}_8 + m_B^2(1-\hat{s})(1-3\hat{s})\mathcal{I}_9\Big]\,. \tag{2.49}$$

In Eqs. (2.40)–(2.49), $v=\sqrt{1-4\hat{m}_\ell^2/\hat{s}}$ is the lepton velocity and

$$\begin{aligned}
A_1=A_1(\hat{s},1/R) &= \frac{-2C_7^{eff}(1/R)}{q^2}\Big(m_b+m_d\Big)g_1(q^2)+(C_9^{eff}(\hat{s},1/R)-C_{10}(1/R))g(q^2)\ ,\\
A_2=A_2(\hat{s},1/R) &= \frac{-2C_7^{eff}(1/R)}{q^2}\Big(m_b-m_d\Big)f_1(q^2)+(C_9^{eff}(\hat{s},1/R)-C_{10}(1/R))f(q^2)\ ,\\
B_1=B_1(\hat{s},1/R) &= \frac{-2C_7^{eff}(1/R)}{q^2}\Big(m_b+m_d\Big)g_1(q^2)+(C_9^{eff}(\hat{s},1/R)+C_{10}(1/R))g(q^2)\ ,\\
B_2=B_2(\hat{s},1/R) &= \frac{-2C_7^{eff}(1/R)}{q^2}\Big(m_b-m_d\Big)f_1(q^2)+(C_9^{eff}(\hat{s},1/R)+C_{10}(1/R))f(q^2)\ ,\\
F=F(1/R) &= 4m_\ell C_{10}(1/R). \qquad (2.50)
\end{aligned}$$

In the above equations, the $\mathcal{I}_i$ have the following representations:

$$\mathcal{I}_i=\int_{-1}^{+1}\mathcal{F}_i(z)dz\ ,$$

where

$$\begin{aligned}
&\mathcal{F}_1=\frac{z^2}{(p_1\cdot k)(p_2\cdot k)}\ ,\quad \mathcal{F}_2=\frac{z}{(p_1\cdot k)(p_2\cdot k)}\ ,\quad \mathcal{F}_3=\frac{1}{(p_1\cdot k)(p_2\cdot k)}\ ,\\
&\mathcal{F}_4=\frac{z^2}{(p_1\cdot k)^2}\ ,\qquad \mathcal{F}_5=\frac{z}{(p_1\cdot k)^2}\ ,\qquad \mathcal{F}_6=\frac{1}{(p_1\cdot k)^2}\ , \qquad (2.51)\\
&\mathcal{F}_7=\frac{z}{(p_2\cdot k)^2}\ ,\qquad \mathcal{F}_8=\frac{z^2}{p_1\cdot k}\ ,\qquad \mathcal{F}_9=\frac{1}{p_1\cdot k}\ .
\end{aligned}$$

3 Numerical results and discussion

In this section, we numerically analyze the physical observables related to the radiative dileptonic $B\to\gamma l^+l^-$ transition both in the ACD and SM models. The main input parameters entering the calculations are form factors. These form factors which we will use in our numerical calculations have been calculated using the light cone QCD sum rules [18, 21–23]:

$$g_(q^2)=\frac{1\ GeV}{\left(1-\frac{q^2}{(5.6\ GeV)^2}\right)^2}\ ,\quad f_(q^2)=\frac{0.8\ GeV}{\left(1-\frac{q^2}{(6.5\ GeV)^2}\right)^2}\ ,$$

$$g_1(q^2)=\frac{3.74\ GeV^2}{\left(1-\frac{q^2}{40.5\ GeV^2}\right)^2}\ ,\quad f_1(q^2)=\frac{0.68\ GeV^2}{\left(1-\frac{q^2}{30\ GeV^2}\right)^2}\ .$$

We also use some other input values to numerically analyze the branching ratios as well as various double—lepton polarization asymmetries: $m_t = 167\ GeV$, $m_W = 80.4\ GeV$, $m_Z = 91.18\ GeV$, $m_c = 1.46\ GeV$, $m_b = 4.8\ GeV$, $m_u = 0.005\ GeV$, $m_B = 5.28\ GeV$, $\alpha_{em} = \frac{1}{137}$, $|V_{tb}V_{td}^*| = 0.01$, $G_F = 1.167 \times 10^{-5}\ GeV^{-2}$, $m_e = 5.1 \times 10^{-4}\ GeV$, $m_\mu = 0.109\ GeV$, $m_\tau = 1.784\ GeV$, and $\tau_B = 1.525 \times 10^{-12} s$.

We start by presenting the results on branching ratios. As we previously noted, in the case of e and μ as final leptons, we only consider the contribution of the structure dependent part to the amplitude. Integrating Eq. (2.33) over $\hat{s}$ in the whole physical region, $4\hat{m_l}^2 \leq \hat{s} \leq 1$ we obtain the total $1/R$-dependent decay width for the $l = e$ or μ. Multiplying this result by the lifetime of the B meson in appropriate unit, we acquire the branching ratio as a function of the compactification factor of extra dimension. As the results of the e and μ channels have similar behavior and are close to each other, we only depict the numerical results in the μ channel. In figure 1, we present the sensitivity of the branching ratio in μ channel on the compactification factor both in the UED and SM models in the interval $200\ GeV \leq 1/R \leq 1000\ GeV$.

Few comments about the lower bound of the compactification scale are in order. Analysis of the $B \to X_s\gamma$ transition and also anomalous magnetic moment had previously shown that the experimental data are in a good consistency with the ACD model if $1/R \geq 300\ GeV$ [30]. From the electroweak precision tests, the lower limit for $1/R$ had also previously been obtained to be 250 GeV if $M_h \geq 250\ GeV$ representing larger KK contributions to the low energy FCNC processes, and 300 GeV if $M_h \leq 250\ GeV$ [7, 31]. Using also the electroweak precision measurements as well as some cosmological constraints, the authors of [32] and [33] have shown that the lower limit on compactification factor is in or above the 500 GeV. Taking into account the leading order (LO) contributions due to the exchange of KK modes together with the available next-to-next-to-leading order (NNLO) corrections to also $B(B \to X_s\gamma)$ decay channel in the SM, the authors of [34] have found a lower bound on the inverse compactification radius as 600 GeV. Finally, using final states with jets and missing transverse momentum, the ATLAS collaboration at CERN is set a 600 GeV on the lower limit of the compactification scale for values of the compression scale between 2 and 40, translating to a lower bound of 730 GeV on the mass of the KK gluon [35]. We will plot the physical observables under consideration in the range $1/R \in [200 - 1000] GeV$ just to clearly show how the results of the UED deviate from those of the SM and grow decreasing the value of $1/R$.

From figure 1 we see that

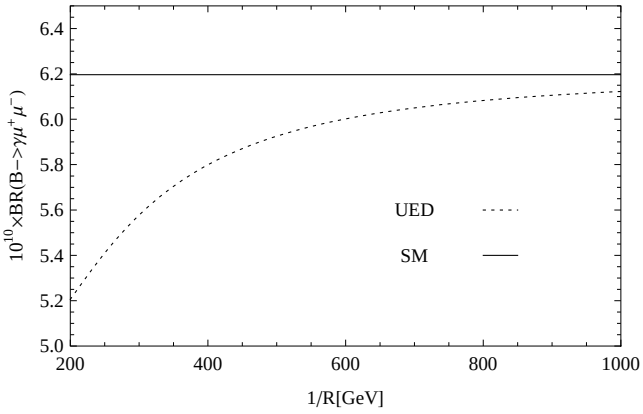

Figure 1: The dependence of the branching ratio for $B \to \gamma\mu^+\mu^-$ on the compactification factor, $1/R$.

- there is a considerable discrepancy between the UED and the SM predictions at lower values of the compactification factor. When $1/R$ is increased the result of UED approaches to that of the SM, such that at upper limit of $1/R$, two models have approximately the same predictions. This discrepancy can be considered as a signal for existing extra dimensions in nature we should look for in hadron colliders.

- Although the contribution of single universal extra dimension has different effects on the Wilson coefficients such that the C_{10} is enhanced and the C_7^{eff} is suppressed (for details see [17]), the branching ratio is suppressed at small values of $1/R$. This is against the effect of the UED in some semileptonic decay channels considered for instance in [12, 17].

- The order of the branching ratios in both models indicate that the predicted results lie below the existing experimental upper limit, $Br(B \to \gamma\mu^+\mu^-) < 1.6 \times 10^{-7}$ [20].

Now, we proceed to depict the results of both UED and SM models on the branching ratio of the $B \to \gamma\tau^+\tau^-$ decay channel. Using the differential decay rate in Eq. (2.34) which contains both the structure-dependent and Bremsstrahlung parts, we obtain the results for branching ratio as shown in figure 2. Here we also see a sizable difference between the predictions of two models at lower values of the compactification factor. Increasing the value of $1/R$ leads to an increase in the value of the branching ratio such that at upper limit, the result of UED becomes roughly the same as the SM. The orders of branching ratios show that the decay channel under consideration is more probable in τ channel case compared to that of the μ. With developments at LHC, we hope we will be able to detect

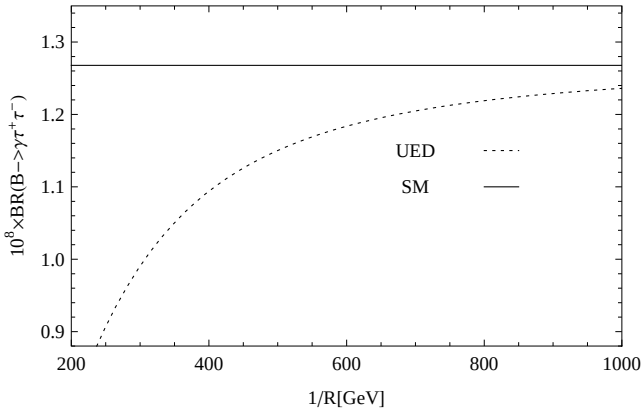

Figure 2: The dependence of the branching ratio for $B \to \gamma\tau^+\tau^-$ on the compactification factor, $1/R$

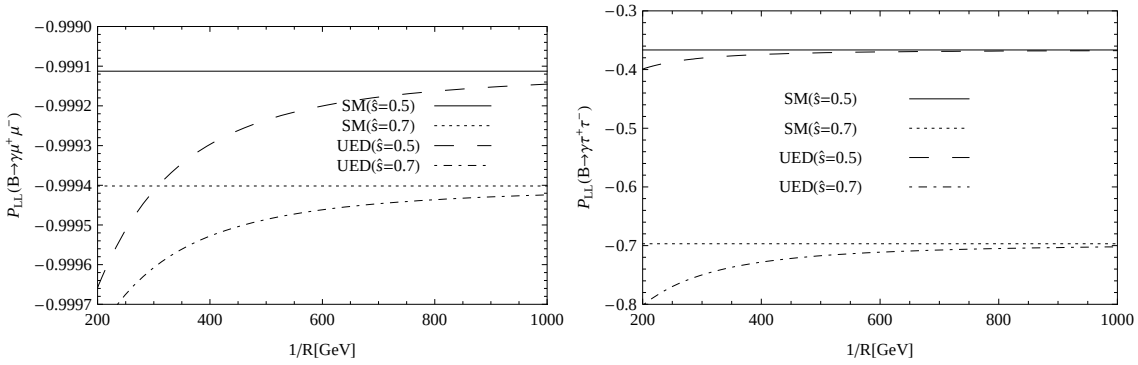

Figure 3: The dependence of the P_{LL} polarization in two models for $B \to \gamma l^+ l^-$ on the compactification factor, $1/R$, for both leptons and at two fixed values of $\hat{s}$.

these channels and determine the exact branching ratios.

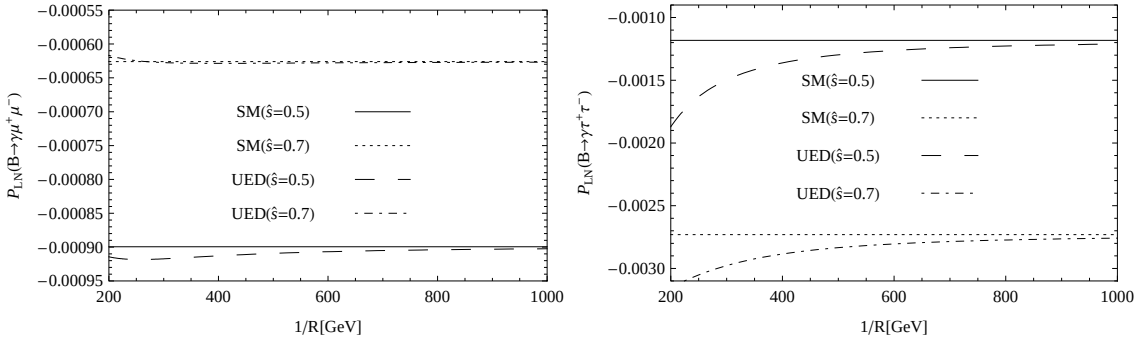

Figure 4: The same as Figure 3, but for P_{LN}.

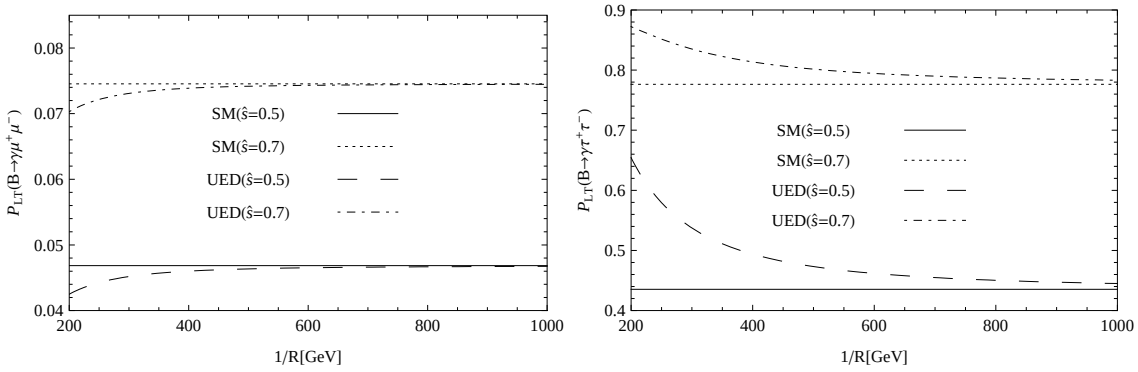

Figure 5: The same as Figure 3, but for P_{LT}.

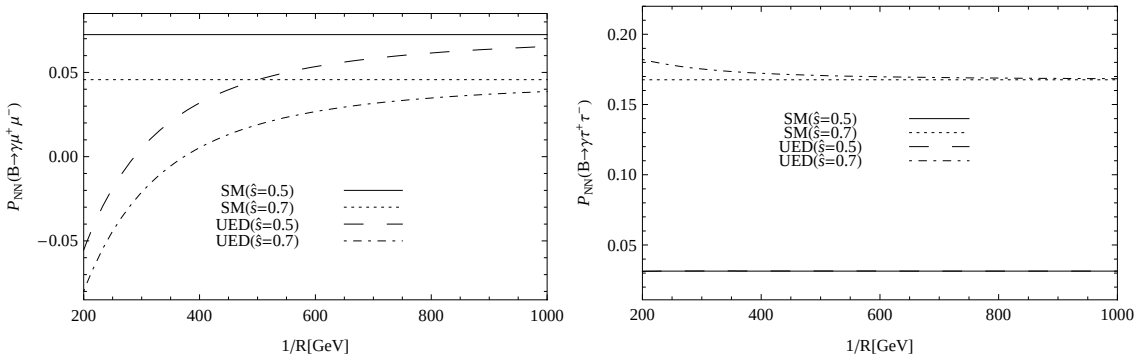

Figure 6: The same as Figure 3 but for P_{NN}

At the end of this section, we would like to show our numerical results on the various double-lepton polarization asymmetries considered in the previous section. For $P_{i\neq j}$, we only show one of the polarizations, not both P_{ij} and P_{ji}. We depict the sensitivity of

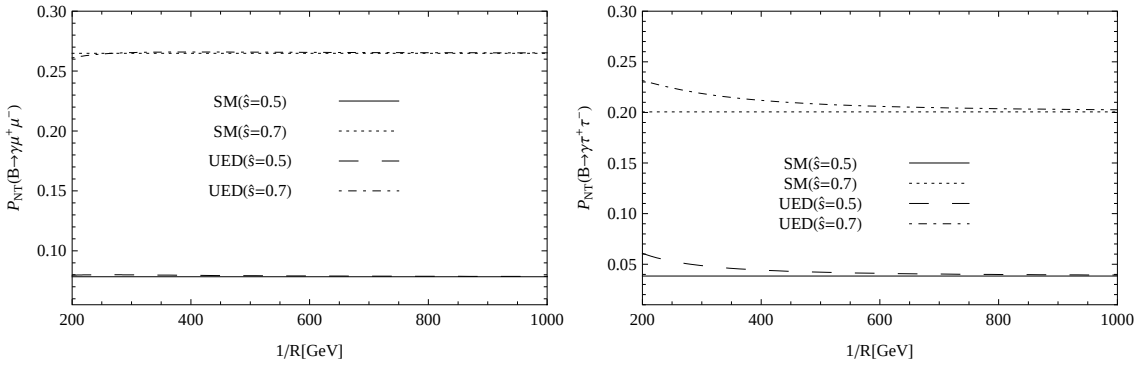

Figure 7: The same as Figure 3, but for P_{NT}

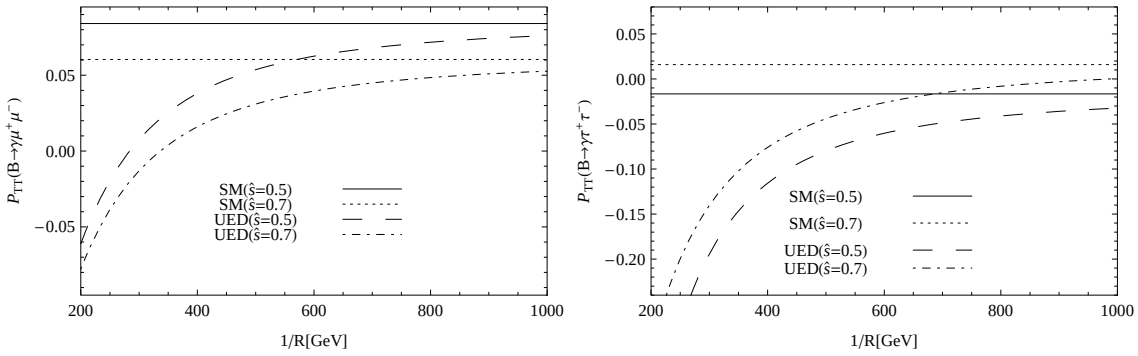

Figure 8: The same as Figure 3, but for P_{TT}

the various double-lepton polarization asymmetries associated with the radiative dileptonic $B \to \gamma l^+ l^-$ decay channel on the compactification factor of extra dimension in figures 3-8. As it is clear from the explicit expressions for the double–lepton polarization asymmetries in the previous section, they have both dependencies on the $1/R$ and the $\hat{s}$. Here, we depict the results for the compactification factor dependence at two fixed values of the $\hat{s}$ in its allowed region. With a quick glance at these figures, we see that

- the polarizations P_{TT}, P_{LT}, P_{LN} and P_{LL} in the τ channel as well as the P_{TT} and P_{NN} in the μ channel show considerable discrepancies between predictions of the two models at lower values of the compactification factor. For the remaining cases, those differences are small.

- Some of the double–lepton polarization asymmetries like P_{TT} in the τ channel are very small in the SM; however take sizable values in the UED model specially at lower values of the compactification factor.

- At a fixed value of $1/R$, we detect strong dependencies on $\hat{s}$ for the P_{LL}, P_{LN}, P_{LT}, P_{NN} and P_{NT} in the τ channel as well as the P_{LN}, P_{LT} and P_{NT} in the μ channel.

Our concluding remark is that any measurement of the physical observables considered in the present study and the comparison of these data with our predictions can give valuable information about the nature of existing extra dimensions.

4 Acknowledgment

We would like to thank T. M. Aliev for useful discussions.

References

[1] I. Antoniadis, Phys. Lett. B 246, 377 (1990).

[2] I. Antoniadis, N. Arkani, S. Dimopoulos, G. Dvali, Phys. Lett. B 439, 257 (1998).

[3] N. Arkani, S. Dimopoulos, G. Dvali, Phys. Lett. B 429, 263 (1998).

[4] N. Arkani, S. Dimopoulos, G. Dvali, Phys. Rev. D 59, 086004 (1999).

[5] L. Randall, R. Sundrum, Phys. Rev. Lett. 83, 3370 (1999).

[6] L. Randall, R. Sundrum, Phys. Rev. Lett. 83, 4690 (1999).

[7] T. Appelquist, H. C. Cheng, B. A. Dobrescu, Phys. Rev. D 64, 035002 (2001).

[8] P. Colangelo, F. De Fazio, R. Ferrandes, T. N. Pham, Phys. Rev. D 73, 115006 (2006).

[9] Yu-Ming Wang, M. J. Aslam, Cai-Dian Lu, Eur. Phys. J. C 59, 847 (2009).

[10] T. M. Aliev, M. Savcı, Eur. Phys. J. C 50, 91 (2007).

[11] B. B. Sirvanli, K. Azizi, Y. Ipekoglu, JHEP 1101, 069 (2011).

[12] K. Azizi, N. Katırcı, JHEP 1101, 087 (2011).

[13] V. Bashiry, M. Bayar, K. Azizi, Phys. Rev. D 78, 035010 (2008).

[14] M.V. Carlucci, P. Colangelo, F. De Fazio, Phys. Rev. D 80, 055023 (2009).

[15] T. M. Aliev, M. Savci, B. B. Sirvanli, Eur. Phys. J. C 52, 375 (2007).

[16] I. Ahmed, M. A. Paracha, M. J. Aslam, Eur. Phys. J. C 54, 591 (2008).

[17] N. Katırcı, K. Azizi, JHEP 1107, 043 (2011).

[18] T. M. Aliev, A. Özpineci, and M.Savcı, Phys. Rev. D 55 (1997) 7059.

[19] T. M. Aliev, N. K. Pak, and M.Savcı, Phys. Lett. B 424 (1998) 175.

[20] K. Nakamura et al. (Particle Data Group), Journal of Physics G37, 075021 (2010).

[21] G. Eilam, I. Halperin and R. R. Mendel, Phys. Lett. B 361, 137 (1995).

[22] T.M. Aliev, A. Ozpineci, M. Savci, Phys. Lett. B 393 (1997) 143.

[23] G. Buchalla and A. J. Buras, Nucl. Phys. B 400 (1993) 225.

[24] A. J. Buras, M. Spranger and A. Weiler, Nucl. Phys. B 660, 225 (2003).

[25] A. J. Buras, A. Poschenrieder, M. Spranger, Nucl. Phys. B 678, 455 (2004).

[26] A. Buras, M. Misiak, M. Münz and S. Pokorski, Nucl. Phys. B 424, 374 (1994).

[27] M. Misiak, Nucl. Phys. B 393, 23 (1993); Erratum ibid B 439, 161 (1995).

[28] B. Buras, M. Münz, Phys. Rev. D 52, 186 (1995).

[29] T. M. Aliev, V. Bashiry, M. Savci, Phys. Rev. D 71 (2005) 035013.

[30] K. Agashe, N. G. Deshpande, G. H. Wu, Phys. Lett. B 514 (2001) 309; B 511 (2001) 85; T. Appelquist, B. A. Dobrescu, Phys. Lett. B 516 (2001) 85.

[31] T. Appelquist, H. U. Yee, Phys. Rev. D 67, 055002 (2003).

[32] I. Gogoladze and C. Macesanu, Phys. Rev. D 74, 093012 (2006).

[33] J. A. R. Cembranos, J. L. Feng and L. E. Strigari, Phys. Rev. D 75, 036004 (2007).

[34] U. Haisch and A. Weiler, Phys. Rev. D 76, 034014 (2007).

[35] ATLAS Collaboration, ATLAS-CONF-2011-155, November 13 (2011).